Phase transitions and bunching of correlated particles in a non-Hermitian quasicrystal

Stefano Longhi [*]

Dipartimento di Fisica, Politecnico di Milano, Piazza L. da Vinci 32, I-20133 Milano, Italy
and IFISC (UIB-CSIC), Instituto de Fisica Interdisciplinar y Sistemas Complejos, E-07122 Palma de Mallorca, Spain

Noninteracting particles in non-Hermitian quasicrystals display localization-delocalization and spectral phase transitions in complex energy plane that can be characterized by point-gap topology. Here we investigate the spectral and dynamical features of two interacting particles in a non-Hermitian quasicrystal, described by an effective Hubbard model in an incommensurate sinusoidal potential with a complex phase, and unravel some intriguing effects without any Hermitian counterpart. Owing to the effective decrease of correlated hopping introduced by particle interaction, doublon states, i.e., bound particle states, display a much lower threshold for spectral and localization-delocalization transitions than single-particle states, leading to the emergence of mobility edges. Remarkably, since doublons display longer lifetimes, two particles initially placed in distant sites tend to bunch and stick together, forming a doublon state in the long time limit of evolution, a phenomenon that can be dubbed *non-Hermitian particle bunching*.

I. INTRODUCTION

Topological phases, localization, and novel phase transitions in non-Hermitian systems with periodic or aperiodic order have recently sparked a great interest in a wide variety of physical systems, ranging from condensed matter physics to cold atoms and classical systems (see, e.g., Refs. [1–13] and references therein). Noninteracting particles in crystalline systems described by an effective non-Hermitian Hamiltonian display a variety of exotic physical effects, such as a nontrivial point-gap topology, the non-Hermitian skin effect, the breakdown of the bulk-boundary correspondence based on Bloch band topological invariants, and a variety of dynamical and transport signatures [14–85]. Recent experimental realizations of synthetic matter with controllable non-Hermitian Hamiltonians using different platforms, such as photonic systems, cold atoms in optical lattices, and mechanical and topolectrical systems, have lead to the observation of such exotic physics.

The study of non-Hermitian physics in such systems is being extended into several directions, unraveling a plethora of intriguing effects which do not have any counterpart in Hermitian systems. For example, in systems with aperiodic order (quasicrystals), non-Hermiticity induces phase transitions that are beyond the paradigm of Hermitian quasicrystals [86–110]. Non-Hermitian extensions of the famous Aubry-André model [111] have attracted great interest recently, unraveling the rich interplay between disorder, non-Hermiticity, and topology. In such systems, the localization-delocalization phase transition and mobility edges in complex energy plane, separating extended and localized states, can be rather generally characterized by point-gap topological numbers [1–12,88,90–93,95–98]. Another interesting ramification is provided by

the many-body physics of noninteracting non-Hermitian systems [112–122], where the construction of many-body states involves ramified symmetry classes leading to unique topological phases. Owing to the different lifetimes of single-particle eigenstates, non-Hermitian many-particle systems may not attain an equilibrium state but rather a nonequilibrium steady state at long times.

Recently, there is a growing focus on exploring non-Hermitian phenomena in *interacting* many-particle systems, aimed at understanding the interplay between non-Hermitian skin effect, interaction, and non-Hermitian topological phases in correlated systems [123–139]. Quantum many-body phases lead to novel manifestations beyond single-particle physics, where the collective behavior of a large number of constituents offers several exotic phases of matter. Among the simplest and intriguing phenomena in strongly correlated quantum systems of both fermions and bosons is the formation of doublons, i.e., pairs of bound particles occupying the same lattice site [140–147]. Such states are readily found within the standard Fermi-Hubbard or Bose-Hubbard models in the two-particle sector of Hilbert space. For sufficiently strong interactions, either attractive or repulsive, isolated doublons represent stable quasiparticles which undergo correlated tunneling on the lattice [148,149]. Doublon dynamics is experimentally accessible using different platforms, such as ultracold atoms in one-dimensional optical lattices [140,148–151], superconducting quantum metamaterials [152], and classical emulators of two- or three-particle dynamics in Fock space based on two- or three-dimensional photonic [153] or topolectrical [154,155] lattices with engineered defects. The current advances in experimental fabrication and control of synthetic matter enables one to extend the few-body Hubbard model into the non-Hermitian realm [155], thus motivating the study of correlated-particle states and doublon dynamics in non-Hermitian models.

*stefano.longhi@polimi.it

In this work we investigate the spectral and dynamical properties of two strongly correlated particles on a lattice in an incommensurate sinusoidal potential with a complex phase [88], i.e., a non-Hermitian extension of the *interacting* Aubry-André model [150], highlighting distinct spectral and localization-delocalization phase transitions for single-particle and doublon states as the complex phase of the incommensurate potential is varied. Specifically, particle interaction introduces mobility edges which are prevented in the single-particle regime and lowers the real-to-complex spectral phase transition owing to the correlated hopping and slow motion of doublons on the lattice. Remarkably, since doublons display longer lifetimes than displaced particle states, two particles initially placed at distant sites of the lattice tend to bunch and stick together, forming a doublon state in the long time limit of evolution. This phenomenon, which can be dubbed the *non-Hermitian bunching effect*, provides an interesting tool for "quantum distillation" of interacting particles [146] of purely non-Hermitian origin.

II. NON-HERMITIAN INTERACTING AUBRY-ANDRÉ MODEL

A. Model

We consider the Hubbard model for interacting fermionic particles in the lowest Bloch band of a one-dimensional tight-binding lattice [156] subjected to an external incommensurate sinusoidal potential, which provides an extension of the Aubry-André model for interacting particles [Fig. 1(a)]. We indicate by J the single-particle hopping amplitude between adjacent sites in the lattice and by U the on-site interaction energy of fermions with opposite spins ($U > 0$ for a repulsive interaction). In the limit $U = 0$ and for an Hermitian potential, the model reduces to the ordinary Aubry-André model. Non-Hermiticity in the system is introduced by considering a complex phase $\varphi = \theta + ih$ of the sinusoidal on-site potential [88], while a reciprocal (Hermitian) amplitude J is assumed for left/right hopping. This means that, contrary to many-body non-Hermitian models considered in several recent works [123–135,137,138], the present model does not display the non-Hermitian skin effect for single-particle states. The effective non-Hermitian Hubbard Hamiltonian of the system reads

$$\hat{H} = -J \sum_{l,\sigma} (\hat{a}_{l,\sigma}^\dagger \hat{a}_{l+1,\sigma} + \text{H.c.}) + \sum_{l,\sigma} V_l \hat{n}_{l,\sigma} + U \sum_l \hat{n}_{l,\uparrow} \hat{n}_{l,\downarrow},$$

$$(1)$$

where $\hat{a}_{l,\sigma}, \hat{a}_{l,\sigma}^\dagger$ are the annihilation and creation operators of fermions with spin $\sigma = \uparrow, \downarrow$ at lattice site l, $\hat{n}_{l,\sigma} = \hat{a}_{l,\sigma}^\dagger \hat{a}_{l,\sigma}$ is the particle-number operator, and

$$V_l = V \cos(2\pi\alpha l + \varphi) - i\gamma \qquad (2)$$

is the complex incommensurate on-site potential with real amplitude V and complex phase

$$\varphi = \theta + ih, \qquad (3)$$

the term $h \geqslant 0$ governing the strength of non-Hermiticity of the system. The positive constant γ provides a uniform loss rate, which just introduces a shift of eigenenergies of the
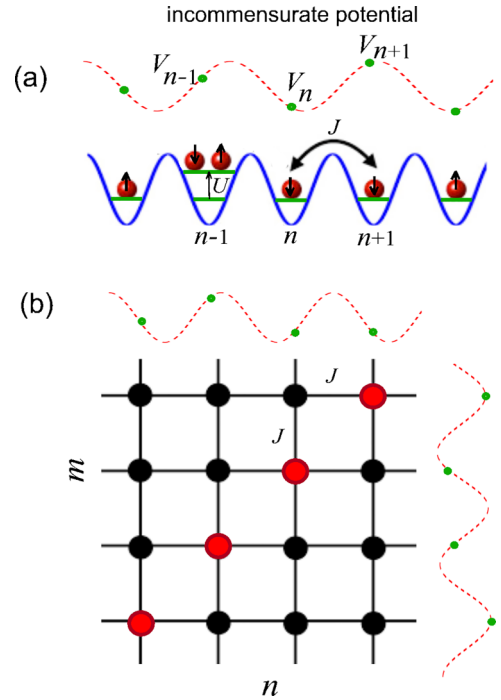
FIG. 1. (a) Non-Hermitian Hubbard model, describing correlated many-particle states in a one-dimensional lattice with a superimposed incommensurate on-site potential (quasicrystal). The reciprocal single-particle hopping rate between adjacent sites is J, U is the on-site interaction energy, and $V_n = V \cos(2\pi\alpha n + \varphi)$ is the incommensurate potential with complex phase $\varphi = \theta + ih$. (b) The Hubbard model for two fermions with opposite spins can be mapped onto the dynamics of a single particle on a square lattice with a line defect on the main diagonal $n = m$ (red circles), corresponding to the interaction energy U, and with a hopping rate J. States bound on the main diagonal $n = m$ in (b) correspond to sticked two-particle states (doublons) in (a). In the strong interaction regime, doublons undergo correlated hopping via a second-order tunneling process with an effective hopping rate $J_e \simeq 2J^2/U$.

system in the complex energy plane along the imaginary axis and avoids instability in a purely dissipative system. Since the specific value of γ does not change the dynamical behavior of the system under continuous measurements, in the following without loss of generality we will assume $\gamma = 0$. As a typical irrational α, we assume the inverse of the golden mean, $\alpha = (\sqrt{5} - 1)/2$, which can be approximated by the sequence of rationals $\alpha = \lim_{n \to \infty} q_n/q_{n+1}$, where q_n are the Fibonacci numbers ($q_0 = 0$, $q_1 = 1$, $q_{n+1} = q_n + q_{n-1}$ for $n \geqslant 1$). In the numerical analysis, we will assume a finite lattice of large size $L = q_{n+1}$ in a ring geometry with periodic boundary conditions ($\hat{a}_{l+L,\sigma} = \hat{a}_{l,\sigma}$) [88].

For pure states and considering open-system dynamics conditioned on measurement outcomes such that the quantum evolution corresponds to the null-jump process, the state vector $|\psi(t)\rangle$ of the system at time t is given by [113–115,124,137,138]

$$|\psi(t)\rangle = \frac{\exp(-i\hat{H}t)|\psi(0)\rangle}{\| \exp(-i\hat{H}t)|\psi(0)\rangle \|} \equiv \frac{|\Phi(t)\rangle}{\| |\Phi(t)\rangle \|}, \qquad (4)$$

where we have set $|\Phi(t)\rangle \equiv \exp(-iHt)|\psi(0)\rangle$. Basically, at each time interval dt the state vector evolves according to the

Schrödinger equation with an effective non-Hermitian Hamiltonian $\hat{H}$, followed by a normalization of the wave function, without undergoing any quantum jump. As mentioned above, under postselection the re-normalization of the wave function after each time interval dt makes it the dynamical evolution of $|\psi(t)\rangle$ independent of the loss rate γ.

B. Single- and two-particle states

The single-particle limit of the Hamiltonian (1), describing the hopping dynamics of a single particle on a one-dimensional incommensurate sinusoidal potential with a complex phase, was earlier introduced Ref. [88]. In this case, when $V < 2J$ a real-to-complex spectral phase transition, corresponding to a delocalization-localization phase transition, is demonstrated to arise as the non-Hermitian parameter h is increased above the critical value [88]

$$h_c = \ln\left(\frac{2J}{V}\right) \tag{5}$$

and can be traced back to the change of a winding number, i.e., to a topological phase transition. For a given base energy E_B, which does not belong to the energy spectrum, one can introduce the winding number w [88]

$$w = \frac{1}{2\pi i} \int_0^{2\pi} d\theta \frac{\partial}{\partial\theta} \ln\left\{\det\left[H\left(\frac{\theta}{L}, h\right) - E_B\right]\right\}, \tag{6}$$

where $H = H(\theta/L, h)$ is the single-particle $L \times L$ matrix Hamiltonian and θ is the real phase angle term entering in the incommensurate potential [Eq. (3)]. The winding number w counts the number of times the complex spectral trajectory encircles the base point E_B when the real phase θ of the potential varies from zero to 2π [1]. When the energy spectrum is entirely on the real energy axis, one clearly has $w = 0$. Conversely, when the energy spectrum describes one or more closed loops in complex plane, for a base energy E_B internal to one of such loops w takes rather generally a nonvanishing integer value, namely one can show that $w = -1$ independent of E_B [88]. Experimental demonstrations of such a kind of non-Hermitian phase transition in quasicrystals, involving a change of the winding number w, have been recently reported in Refs. [109,110].

In this work we will focus our analysis on considering two fermions with opposite spins hopping on the one-dimensional lattice. In this case, we can expand the state vector $|\psi(t)\rangle$ of the system in Fock space according to

$$|\psi(t)\rangle = \sum_{n,m} \psi_{n,m}(t) \hat{a}^\dagger_{n,\uparrow} \hat{a}^\dagger_{m,\downarrow} |0\rangle. \tag{7}$$

Note that the probability of finding the two particles at the same site n is given by $P_n(t) = |\psi_{n,n}(t)|^2$. After letting $\psi_{n,m}(t) = \Phi_{n,m}(t)/\sqrt{\sum_{n,m}|\Phi_{n,m}(t)|^2}$, the evolution equations for the amplitudes $\Phi_{n,m}(t)$ are readily obtained from the Schrödinger equation of a pure state with the effective non-Hermitian Hamiltonian $\hat{H}$ given by Eq. (1) and read

$$i\frac{d\Phi_{n,m}}{dt} = -J(\Phi_{n,m+1} + \Phi_{n,m-1} + \Phi_{n+1,m} + \Phi_{n-1,m})$$
$$+ U\delta_{n,m}\Phi_{n,m} + (V_n + V_m)\Phi_{n,m}. \tag{8}$$

Equation (8) shows that the hopping dynamics of the two interacting fermions on a one-dimensional lattice is basically equivalent to the hopping motion of a single particle in a two-dimensional square lattice with an incommensurate on-site potential and with an additional defect line on the main diagonal $m = n$, under the periodic boundary conditions $\Phi_{n+L,m} = \Phi_{n,m+L} = \Phi_{n,m}$ [see Fig. 1(b)]. Therefore, the spectral and localization properties as well as the dynamical motion of two-particle states in the original one-dimensional quasicrystal can be readily understood by considering the single-particle states in a two-dimensional quasicrystal with a defect line on the main diagonal. Finally, we mention that, while our analysis considers two interacting fermions with opposite spins, in the two-particle sector of Hilbert space the Hubbard model Eq. (1) can also describe the dynamical evolution of two identical bosonic particles (rather than two distinct fermions), with the only additional constraint being the symmetrization of the wave function under particle exchange.

III. SPECTRAL AND LOCALIZATION-DELOCALIZATION PHASE TRANSITIONS

Let us indicate by $\psi_{n,m}^{(\beta,\delta)} \equiv |\psi^{(\beta,\delta)}\rangle$ and $E_{\beta,\delta}$ the two-particle eigenstates and corresponding eigenenergies of the $L^2 \times L^2$ matrix Hamiltonian corresponding to $\hat{H}$ in the two-particle sector of Hilbert space, where $\beta, \delta = 1, 2, \ldots, L$ is a pair of indices labeling the matrix eigenstates. Here we aim at exploring the impact of particle interaction on the spectral and localization-delocalization phase transitions found in the single-particle case. For $h > 0$, the energy spectrum is rather generally described by energies in complex plane and a transition from an entirely real to complex spectrum can be detected by monitoring the behavior of $\epsilon \equiv \max_{\beta,\delta}|\text{Im}(E_{\beta,\delta})|$ versus the non-Hermitian complex phase h. The localization features of the eigenstates are captured by the inverse participation ratio (IPR), defined by

$$\text{IPR}^{(\beta,\delta)} = \frac{\sum_{n,m=1}^{L}\left|\psi_{n,m}^{(\beta,\delta)}\right|^4}{\left(\sum_{n,m=1}^{L}\left|\psi_{n,m}^{(\beta,\delta)}\right|^2\right)^2}. \tag{9}$$

The IPR of an extended state scales as L^{-2}, hence vanishing in the $L \to \infty$ limit, while it remains finite for a localized state, with IPR $\leqslant 1$ and IPR $= 1$ when the excitation occupies a single site. In the following, we will indicate by $\text{IPR}_{\text{max}} \equiv \max_{\beta,\delta}\text{IPR}^{(\beta,\delta)}$ and $\text{IPR}_{\text{min}} \equiv \min_{\beta,\delta}\text{IPR}^{(\beta,\delta)}$ the largest and smallest values of IPR over the eigenstates of the Hamiltonian. For a given base energy E_B that does not belong to the energy spectrum, a winding number w can be introduced, which measures the times the complex two-particle energy spectrum rotates around E_B when the angle θ adiabatically varies from 0 to 2π. The definition of w is basically the same as Eq. (6), where now $H(\theta/L, h)$ is the matrix associated to $\hat{H}$ in the two-particle sector of Hilbert space. Since the energy spectrum in complex energy plane is described by multiple layers of closed loops in complex energy plane [see, for example, Figs. 2(d), 3(d), 4(d), and 5(d) discussed below], whose number increases with the system size L, the winding number w is size dependent and can take large values, i.e., not
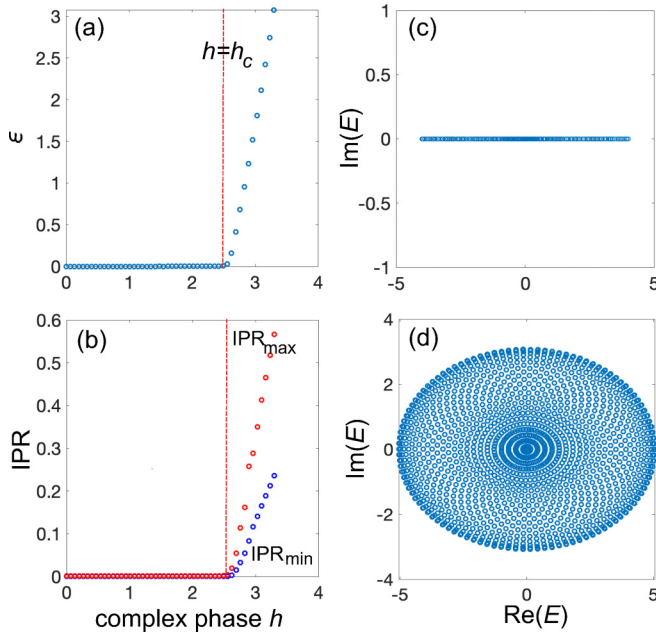
FIG. 2. Two-particle energy spectrum and IPR of eigenstates in the noninteracting limit $U = 0$. Other parameter values are $J = 1$, $V = 0.15$, $\theta = 0$, $\alpha = 34/55$, and $L = 55$. (a) Behavior of the largest value ϵ (in modulus) of the imaginary part of any eigenenergy versus the complex phase h of the incommensurate potential. The vertical dashed line corresponds to the spectral phase transition point $h = h_c = \ln(2J/V) \simeq 2.59$. (b) Behavior of the largest and smallest values of the IPR versus h. [(c),(d)] Energy spectra in complex energy plane for $h = 1$ [panel (c)] and $h = 3.3$ [panel (d)]. In (d) the spectrum comprises multiple layers of closed loops in complex plane, characterized by a nonvanishing winding number w for any base energy E_B internal to such loops. For example, for the base energies $E_B = 0, 1.5$, and 2.5, one has $w = -55, -45$, and -37, respectively.

limited to $w = 0, -1$ [128]. For a sufficiently large system size L and E_B not too close to any energy in the spectrum, as previously discussed in Ref. [128] the function under the sign of the integral in Eq. (6) is almost independent of θ and, thus, after letting

$$\det\left\{ H\left(\frac{\theta}{L}, h\right) - E_B \right\} \equiv R(\theta) \exp[i\omega(\theta)],$$

one can simply calculate the winding number using the relation

$$w(E_B) \simeq \frac{d\omega}{d\theta} \qquad (10)$$

at any arbitrary value of the angle θ. It should be mentioned that, while in the single-particle case the winding number is defined taking the $L \to \infty$ limit [88], for two-particle states one should keep the system size L finite since in the limit $L \to \infty$ the number of closed loops diverges and the energy spectrum covers an entire area (rather than a numerable set of curves).

In the noninteracting limit $U = 0$, the two-particle eigenstates $\psi_{n,m}^{(\beta,\delta)}$ and corresponding eigenenergies $E_{\beta,\delta}$ are readily obtained from the single-particle spectral properties of $\hat{H}$;
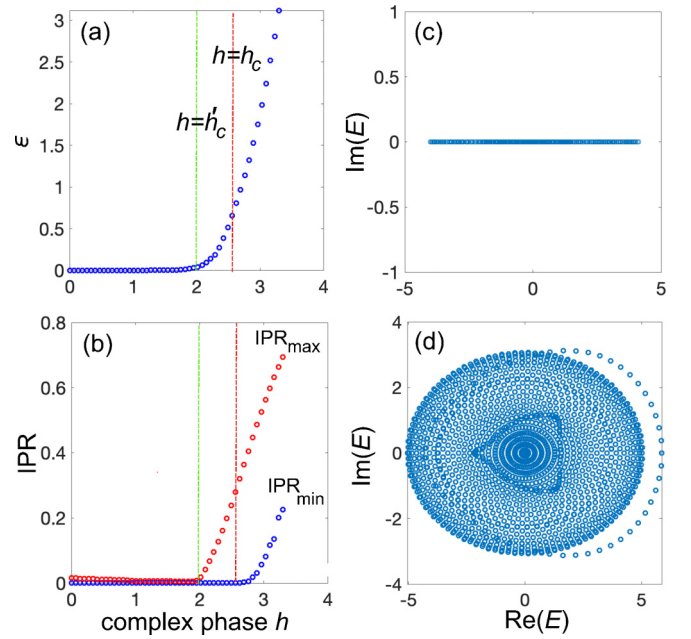
FIG. 3. Same as Fig. 2, but for $U = 1$. Note that the real-to-complex spectral phase transition is observed at a lower value h'_c of the complex phase than h_c. The value h'_c corresponds to the appearance of localized eigenstates, indicated by a finite value of IPR_{max}. For $h < h'_c$ all eigenstates are extended, for $h'_c < h < h_2$ with $h_2 \simeq h_c$ localized and extended states coexist, whereas for $h > h_2$ all eigenstates are localized.

namely one has

$$\psi_{n,m}^{(\beta,\delta)} = \psi_n^{(\beta)} \psi_m^{(\delta)} \qquad (11)$$

and

$$E_{\beta,\delta} = E_\beta + E_\delta, \qquad (12)$$
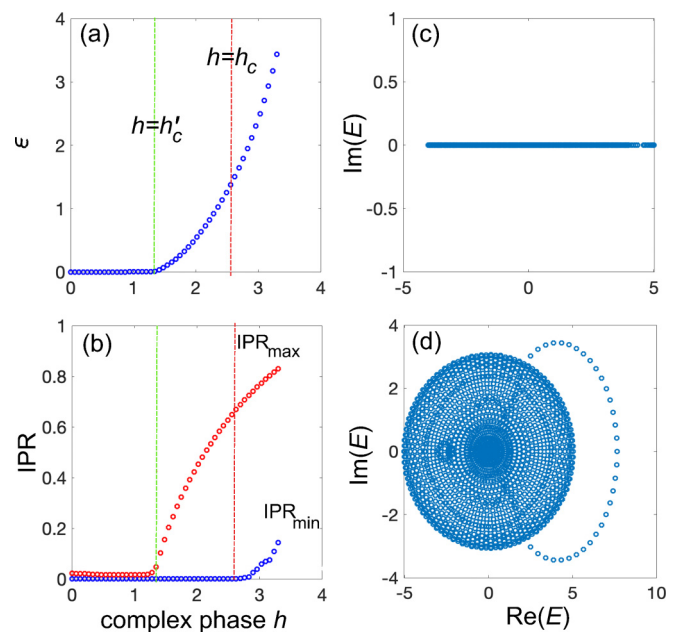
FIG. 4. Same as Fig. 3, but for $U = 3$.
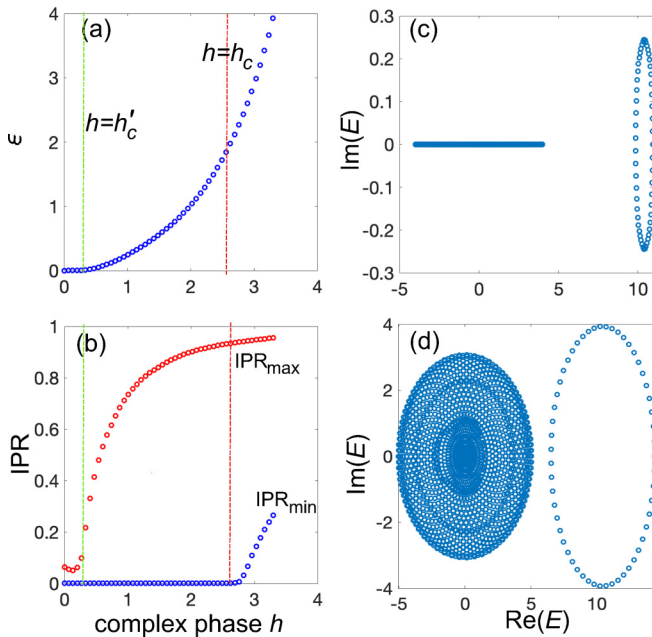
FIG. 5. Same as Fig. 3, but for $U = 10$.

where E_β and $\psi_n^{(\beta)}$ are the eigenenergies and corresponding eigenstates of the single-particle Hamiltonian

$$E_\beta \psi_n^{(\beta)} = -J\left(\psi_{n+1}^{(\beta)} + \psi_{n-1}^{(\beta)}\right) + V \cos(2\pi\alpha n + \varphi)\psi_n^{(\beta)}. \quad (13)$$

In this case, for $h < h_c$ the energy spectrum remains entirely real and all eigenstates are delocalized, whereas for $h > h_c$ the energy spectrum becomes complex, composed by multiple layers of closed loops in complex energy plane, with simultaneous localization of all corresponding eigenstates. As an example, Figs. 2(a) and 2(b) show the behavior of ϵ and of $\text{IPR}_{\text{max,min}}$ versus h, as obtained by numerical diagonalization of the two-particle matrix Hamiltonian, for noninteracting two-particle states in a lattice with parameter values $\alpha = q_n/q_{n+1} = 34/55$, lattice size $L = q_{n+1} = 55$, hopping amplitude $J = 1$, potential amplitude $V = 0.15$, and phase $\theta = 0$. Clearly, for $h < h_c = \ln(2J/V) \simeq 2.59$, all eigenstates are delocalized and the energy spectrum is real, whereas for $h > h_c$ the energy spectrum becomes complex and all eigenstates become simultaneously localized. Figures 2(c) and 2(d) show typical energy spectra in the $h < h_c$ and $h > h_c$ phases, respectively. Note that for $h > h_c$ the energy spectrum includes multiple layers of loops in complex plane. Such a layered structure is typical of two-particle states, does not actually require interaction, and, as a distinctive feature from single-particle states, leads to a winding number w which is system-size dependent and can take large values, depending on the numbers of loops in the layer (see, e.g., Ref. [128]). For example, for the case of Fig. 2(d) with $L = 55$ the winding number w takes the values $w = -55$, -45, and -37 for a base energy $E_B = 0$, 1.5, and 2.5, respectively.

The spectral and localization properties of the system for increasing values of interaction energy U are shown in Figs. 3, 4, and 5. The effects arising from particle interaction are mainly twofold. First, one clearly sees a lowering of the threshold value h'_c for the real-to-complex spectral phase

transition from the value h_c predicted in the single-particle case [Eq. (5)]. Second, when the complex phase h varies in the range $h'_c < h < h_2$, with $h_2 \sim h_c$, extended and localized states coexist, as one can infer from the inspection of the IPR_{min}, which remains close to zero indicating the existence of extended states, and IPR_{max}, which takes finite values corresponding to localized states. Therefore, interaction leads to the appearance of mobility edges, which are prevented in the single-particle (noninteracting) case. Extended and localized states correspond to real and complex energies, respectively. Interestingly, as the interaction energy U increases one loop in the cluster of Fig. 2(d) detaches and separates with the formation of a line gap from the other layers, as shown in Figs. 3(d), 4(d) and 5(d). For $h > h_2$, deformation of the energy loop layers induced by energy interaction changes rather generally the values of winding numbers w as compared to the noninteracting limit. For example, for the case of Fig. 5(d) one has $w = -54$, -43, and -36 at the base energies $E_B = 0$, 1.5, and 2.5, respectively (to be compared with the values of w given in Fig. 1).

The loop detachment observed as U increases is analogous to the formation of the Mott-Hubbard gap in the standard (Hermitian) Hubbard model in strongly correlated systems. The detached loop basically describes doublon states, i.e., sticked two-particle states which undergo correlated hopping along the lattice. In the single-particle analog shown in Fig. 1(b), doublon dynamics and correlated particle hopping basically correspond to bound excitations near the defective line along the main diagonal in the square lattice, which cannot spread in the lattice bulk owing to energy conservation constraint. The doublon dynamics can be described in the strong-interaction limit $U \gg J, V \exp(h)$ by a reduced model obtained from a multiple time scale analysis of Eq. (8), which is detailed in Appendix A. After letting $\Phi_{n,n}(t) = A_n(t)\exp(-iUt)$, one obtains the following evolution equations for the slowly varying amplitudes A_n, corresponding to the amplitude probabilities that the two particles are found at the same lattice site n at time t:

$$i\frac{dA_n}{dt} = J_e(A_{n+1} + A_{n-1} + 2A_n) + 2V_nA_n, \quad (14)$$

where

$$J_e \equiv \frac{2J^2}{U} \quad (15)$$

is the effective (second-order) hopping rate of the sticked two-particle state (doublon). Basically, the hopping rate of J_e for doublons, being a second-order process, is greatly reduced as compared to the hopping rate J of a single particle, which corresponds to an effective increase of the amplitude of the incommensurate non-Hermitian potential for doublons. This explains the lowering of the real-to-complex spectral phase transition observed as the interaction energy U is increased, from the single-particle value h_c to the lower value h'_c, which can be estimated in the strong interaction limit using Eq. (14), yielding

$$h'_c \simeq \ln\left(\frac{J_e}{V}\right) = \ln\left(\frac{2J^2}{UV}\right) = h_c - \ln\left(\frac{U}{J}\right). \quad (16)$$

In particular, when the interaction energy U is larger than the critical value $U_c = 2J^2/V$, one has $h'_c = 0$, i.e., the energy spectrum becomes immediately complex as soon as the potential is complex.

IV. CORRELATED DYNAMICS AND NON-HERMITIAN PARTICLE BUNCHING

In the Hermitian limit of the Hubbard model considered in the previous section two fermions that are initially placed at different sites in the lattice do not tend to bunch and stick together owing to energy repulsion. Likewise, two fermions initially prepared in the same lattice site form a doublon that undergoes correlated hopping on the lattice, i.e., particle dissociation is prevented owing to energy conservation. In the many-particle case where lattice sites can be singly or doubly occupied, the slow motion of doublons as compared to single particle occupancies can be harnessed to realize "quantum distillation," i.e., to separate doublons from singlons [146].

The particle dynamics is deeply modified when considering the non-Hermitian extension of the Hubbard model. In fact, the correlated particle dynamics on the lattice in the non-Hermitian regime $h > h'_c$ is greatly influenced by the different "lifetimes," i.e., imaginary parts of eigenenergies, of doublon states than single-particle states. Since doublons display longer lifetimes, in the strong interaction regime a rather arbitrary initial excitation of the system, that is not exactly orthogonal to doublon eigenstates, is attracted toward one of such eigenstates in the long time limit, i.e., the two particles tend to bunch and stick together as a result of the non-Hermitian dynamics, a phenomenon that can be referred to as *non-Hermitian particle bunching*. We note such a phenomenon is distinct from quantum distillation of doublons and singlons observed in the Hermitian case and briefly mentioned above, where single-particle states move faster than doublons and can escape from the edges of the system [146].

To understand the non-Hermitian bunching effect, let us observe that for a given initial condition the state of the system at time t can be written as

$$|\psi(t)\rangle = \frac{\sum_{\beta,\delta} C_{\beta,\delta}|\psi^{(\beta,\delta)}\rangle \exp(-iE_{\beta,\delta}t)}{\|\sum_{\beta,\delta} C_{\beta,\delta}|\psi^{(\beta,\delta)}\rangle \exp(-iE_{\beta,\delta}t)\|}, \qquad (17)$$

where the spectral amplitudes $C_{\beta,\delta}$ are determined by the initial state $|\psi(0)\rangle$ and are given by

$$C_{\beta,\delta} = \langle\psi^{\dagger(\beta,\delta)}|\psi(0)\rangle. \qquad (18)$$

In the above equation, $\psi^{\dagger(\beta,\delta)}$ are the eigenfunctions of the adjoint Hamiltonian $\hat{H}^\dagger$ in the two-particle sector of Hilbert space, which is obtained from $\hat{H}$ by just reversing the sign of h, and the orthonormal conditions $\langle\psi^{\dagger(\beta,\delta)}|\psi^{(\beta',\delta')}\rangle = \delta_{\beta,\beta'}\delta_{\delta,\delta'}$ are assumed. From Eq. (17), it then follows that the long-time dynamics of the system is dominated by the excited two-particle eigenstate of $\hat{H}$ with the largest imaginary part of the eigenenergy, which is expected to be rather generally a doublon eigenstate.

As an example, let us assume that at initial time $t = 0$ the two particles are initially placed at sites n_1 and n_2 of the lattice, distant from one another by $d = |n_2 - n_1|$, and let us consider the symmetrized wave function as an initial state

$$|\psi(0)\rangle = \frac{1}{\sqrt{2}}\left(\hat{a}^\dagger_{n_1,\uparrow}\hat{a}^\dagger_{n_2,\downarrow}|0\rangle + \hat{a}^\dagger_{n_2,\uparrow}\hat{a}^\dagger_{n_1,\downarrow}|0\rangle\right) \qquad (19)$$

(symmetrization of the wave function is assumed so as to include in the analysis the case of two bosonic particles as well). The probability that at time t the two particles stick together (bunching probability) is computed from the relation

$$P_{\text{bun}}(t) = \sum_n |\psi_{n,n}(t)|^2. \qquad (20)$$

Figure 6 shows the numerically computed temporal evolution of the site occupation probabilities of the two particles on the lattice, initially placed at a distance $d = 1$ form one another, for the same parameter values as in Fig. 5 ($J = 1$, $L = 55$, $\alpha = 34/55$, $V = 0.15$, and $\theta = 0$) in the Hermitian ($h = 0$, upper row) and non-Hermitian ($h = 1$, lower row) regimes, clearly indicating that in the latter case the two particles tend to stick together, while in the former case they do not. The corresponding behavior of the bunching probability is shown in Fig. 7(a). The time required for the two particles to bunch together is clearly dependent on the lifetime differences between doublon and single-particle eigenstates and on the weight $|C_{\beta,\delta}|$ of the overlapping of initial state onto the doublon eigenstate with the largest growth rate, which decreases as the particle distance d increases. Hence the time of the two particles to stick together increases as d is increased; compare, e.g., Figs. 7(a) and 7(b), where the initial distance d of the two particles is increased from $d = 1$ to $d = 2$. Quantitatively, we can define a bunching time τ_0 such that $P_{\text{bun}}(\tau_0)$ reaches a target (reference) value, for example 80%. A typical behavior of τ_0 versus initial particle separation d is shown in Fig. 7(c), indicating that τ_0 increases almost linearly with d.

V. CONCLUSIONS

Topological phases and phase transitions in non-Hermitian crystalline or quasicrystalline systems provide a fascinating area of research with promising implications in different fields of physics, from condensed matter to cold atoms and classical systems such as photonic, acoustic, mechanical, and topolectrical settings. While the properties of single-particle non-Hermitian models have been the subject of extensive studies and revealed unprecedented phenomena without any counterpart in Hermitian systems, such as the appearance of nontrivial point-gap and line-gap topologies, the non-Hermitian skin effect, an extended form of the bulk-boundary correspondence, and a variety of dynamical and transport effects, intriguing physical phenomena are being discovered when considering interacting many-body non-Hermitian systems. In this work we investigated the spectral and dynamical features of two interacting particles in a non-Hermitian quasicrystal, described by an effective Hubbard model in an incommensurate sinusoidal potential with a complex phase, and unravelled some intriguing effects without any Hermitian counterpart. Owing to an effective increase of disorder strength introduced by particle interaction, doublon states, i.e., bound particle states, display a much lower threshold for spectral and localization-delocalization transitions than
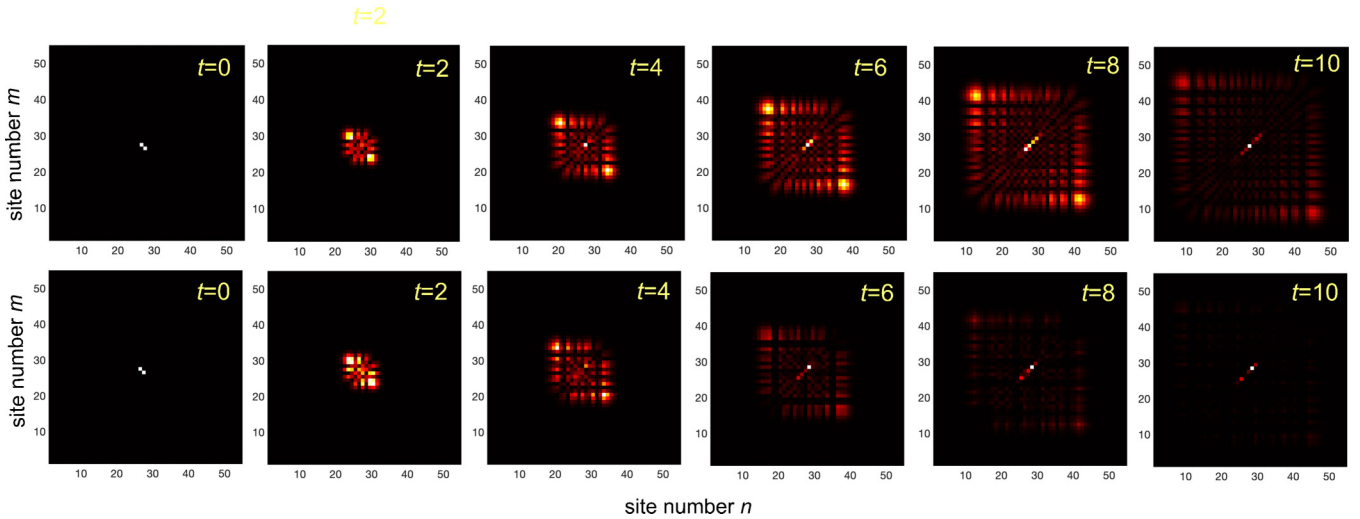
FIG. 6. Temporal evolution of the two-particle probability distributions $|\psi_{n,m}(t)|^2$ in a lattice with the same parameter values as in Fig. 5 ($J = 1, U = 10, V = 0.15, L = 55, \theta = 0$) and for $h = 0$ (Hermitian limit, upper row) and $h = 1$ (lower row). The system is initially prepared in a symmetrized state with one particle at site $n_1 = 26$ and the other one at site $n_2 = 27$.

single-particle states, leading to the formation of interaction-induced mobility edges. Remarkably, since doublons display longer lifetimes, two particles initially placed at distant sites in the lattice tend to bunch and stick together, forming a doublon state in the long time limit of evolution, a phenomenon that can be dubbed *non-Hermitian particle bunching*. Our results shed light onto the physical properties of strongly correlated particles in non-Hermitian systems, even in the few-body case considered here, and could suggest possibilities to control many-particle states harnessing non-Hermitian physics. In the present study, the analysis has been focused on a specific non-Hermitian interacting Aubry-André model, where non-Hermiticity enters via a complex phase h in the incommensurate on-site potential; however, different non-Hermitian versions of the interacting Aubry-André model could be considered, such as the Aubry-André model with off-diagonal incommensurate disorder [91,106] or the Aubry-André model with nonreciprocal (asymmetric) hopping amplitudes [92,95,97] induced by an imaginary magnetic flux η [157], which displays the non-Hermitian skin effect

in the single-particle regime [5,7,12]. In particular, it would be interesting to investigate the interplay and competition between complex phase h of the incommensurate potential, which tends to localize the wave functions, and the magnetic flux η, which tends to delocalize the wave functions and plays the same role as h but in reciprocal (Fourier) space [88]. Since the imaginary magnetic flux η acts in a different way for two-particle scattered states and two-particle bound states (doublons) [158], the non-Hermitian bunching effect is expected to be washed out by the imaginary magnetic flux and doublon dissociation in the bulk would be observed for a magnetic flux η larger than the complex phase h.
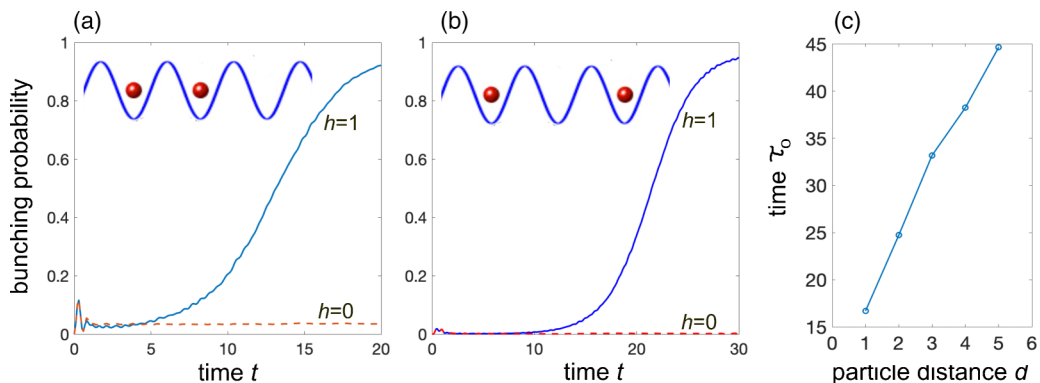
FIG. 7. (a) Temporal evolution of the bunching probability for the same parameter values as in Fig. 6 for $h = 0$ (Hermitian limit, dotted curve) and $h = 1$ (solid curve). (b) Same as (a), but for an initial separation of the two particles $d = 2$. (c) Behavior of the bunching time τ_0 versus initial particle distance d for $h = 1$. τ_0 is defined such that $P_{\text{bun}}(\tau_0) = 0.8$.

APPENDIX: DOUBLON DYNAMICS: MULTIPLE-TIME SCALE ANALYSIS

In this Appendix we derive Eqs. (14) and (15) given in the main text, which describe the correlated hopping of two particles in the lattice that occupy the same site at each time (doublons). Let us introduce the normalized time variable $\tau = Ut$, so that Eq. (8) take the form

$$i\frac{d\Phi_{n,m}}{d\tau} = -\frac{J}{U}(\Phi_{n,m+1} + \Phi_{n,m-1} + \Phi_{n+1,m} + \Phi_{n-1,m})$$
$$+ \delta_{n,m}\Phi_{n,m} + \frac{V_n + V_m}{U}\Phi_{n,m}. \quad \text{(A1)}$$

Let us now consider the strong interaction regime by assuming $J/U \equiv \epsilon$, with $\epsilon \ll 1$. We also consider a potential strength V and complex phase h such that $U \gg V\exp(h)$, with $V\exp(h)/U \sim \epsilon^2$. Therefore, in Eq. (A1) the first term on the right hand side of the equation is of order $\sim\epsilon$, the second term is of order $\sim\epsilon^0$, and the last term is of order $\sim\epsilon^2$. Let us now assume that at initial time the system is prepared in a doublonic state, i.e., such that $\Phi_{n,m}(\tau=0) = 0$ for $n \neq m$, and let us look for a solution to Eq. (A1) as an asymptotic series

$$\Phi_{n,m}(\tau) = \Phi_{n,m}^{(0)}(\tau) + \epsilon\Phi_{n,m}^{(1)}(\tau) + \epsilon^2\Phi_{n,m}^{(2)}(\tau) + \cdots. \quad \text{(A2)}$$

To ensure that the expansion (A2) is uniformly valid as τ grows, multiple time scales

$$T_0 = \tau, \quad T_1 = \epsilon\tau, \quad T_2 = \epsilon^2\tau, \dots \quad \text{(A3)}$$

have to be introduced to avoid the occurrence of secular growing terms in the asymptotic expansion. Using the derivative rule

$$\frac{d}{d\tau} = \frac{d}{dT_0} + \epsilon\frac{d}{dT_1} + \epsilon^2\frac{d}{dT_2} + \cdots, \quad \text{(A4)}$$

substitution of Eqs. (A2) and (A4) into Eq. (A1), and after equating terms of the same power in ϵ, a hierarchy of equations for successive corrections to $\Phi_{n,m}$ is obtained. At leading order $\sim\epsilon^0$ one simply obtains

$$i\frac{\partial\Phi_{n,m}^{(0)}}{\partial T_0} = \delta_{n,m}\Phi_{n,m}^{(0)}, \quad \text{(A5)}$$

which can be readily solved by letting

$$\Phi_{n,m}^{(0)} = A_n\delta_{n,m}\exp(-iT_0), \quad \text{(A6)}$$

where the amplitudes A_n can vary on the slow time scales $T_1, T_2, \dots$, i.e., $A_n = A_n(T_1, T_2, \dots)$. At order $\sim\epsilon$ one has

$$i\frac{\partial\Phi_{n,m}^{(1)}}{\partial T_0} = -(\Phi_{n+1,m}^{(0)} + \Phi_{n-1,m}^{(0)} + \Phi_{n,m+1}^{(0)} + \Phi_{n,m-1}^{(0)}) \quad \text{(A7)}$$

for $n \neq m$ and

$$i\frac{\partial\Phi_{n,n}^{(1)}}{\partial T_0} - \Phi_{n,n}^{(1)} = -i\frac{\partial A_n}{\partial T_1}\exp(-iT_0). \quad \text{(A8)}$$

The solvability condition for Eq. (A8) yields

$$\frac{\partial A_n}{\partial T_1} = 0, \quad \Phi_{n,n}^{(1)} = 0, \quad \text{(A9)}$$

whereas Eq. (A7) can be solved for $\Phi_{n,m}^{(1)}$ ($n \neq m$), yielding

$$\Phi_{n,m}^{(1)} = -(A_{n+1}\delta_{m,n+1} + A_{n-1}\delta_{m,n-1} + A_n\delta_{m,n+1} + A_n\delta_{m,n-1})\exp(-iT_0). \quad \text{(A10)}$$

Finally, at order $\sim\epsilon^2$ for $n = m$ one obtains

$$i\frac{\partial\Phi_{n,n}^{(2)}}{\partial T_0} - \Phi_{n,n}^{(2)} = \exp(-iT_0)\left\{ -i\frac{\partial A_n}{\partial T_2} + \frac{2V_n}{\epsilon^2 U}A_n \right.$$
$$\left. + 2(A_{n+1} + A_{n-1} + 2A_n) \right\}. \quad \text{(A11)}$$

The solvability condition to Eq. (A11) yields

$$i\frac{\partial A_n}{\partial T_2} = \frac{2V_n}{\epsilon^2 U}A_n + 2(A_{n+1} + A_{n-1} + 2A_n). \quad \text{(A12)}$$

If we stop the asymptotic analysis at order $\sim\epsilon^2$, after reintroduction of the original variables from Eqs. (A2), (A4), (A6), (A9), and (A12) one finally obtains

$$\Phi_{n,n}(t) = A_n(t)\exp(-iUt) + O(\epsilon^2),$$
$$\Phi_{n,m}(t) = O(\epsilon) \quad (m = n \pm 1), \quad \text{(A13)}$$
$$\Phi_{n,m}(t) = o(\epsilon) \quad (|m - n| \geqslant 2),$$

where the slowly varying amplitudes A_n evolve according to the following equations:

$$i\frac{dA_n}{dt} = \frac{2J^2}{U}(A_{n+1} + A_{n-1} + 2A_n) + 2V_nA_n, \quad \text{(A14)}$$

which correspond to Eqs. (14) and (15) given in the main text, with $J_e \equiv 2J^2/U$. Note that J_e corresponds to an effective hopping rate of two-particle states, which is a second-order process (as it arises at order $\sim\epsilon^2$ in the asymptotic analysis).

[1] Z. Gong, Y. Ashida, K. Kawabata, K. Takasan, S. Higashikawa, and M. Ueda, Topological Phases of Non-Hermitian Systems, Phys. Rev. X **8**, 031079 (2018).

[2] A. Ghatak and T. Das, New topological invariants in non-Hermitian systems, J. Phys.: Condens. Matter **31**, 263001 (2019).

[3] K. Kawabata, K. Shiozaki, M. Ueda, and M. Sato, Symmetry and Topology in Non-Hermitian Physics, Phys. Rev. X **9**, 041015 (2019).

[4] L. E. F. Foa Torres, Perspective on topological states of non-Hermitian lattices, J. Phys. Mater. **3**, 014002 (2020).

[5] E. J. Bergholtz, J. C. Budich, and F. K. Kunst, Exceptional topology in non-Hermitian systems, Rev. Mod. Phys. **93**, 015005 (2021).

[6] Y. Ashida, Z. Gong, and M. Ueda, Non-Hermitian physics, Adv. Phys. **69**, 249 (2020).

[7] X. Zhang, T. Zhang, M.-H. Lu, and Y.-F. Chen, A review on non-Hermitian skin effect, Adv. Phys. X **7**, 2109431 (2022).

[8] K. Ding, C. Fang, and G. Ma, Non-Hermitian topology and exceptional-point geometries, Nat. Rev. Phys. **4**, 745 (2022).

[9] A. Banerjee, R. Sarkar, S. Dey, and A. Narayan, Non-Hermitian topological phases: Principles and prospects, J. Phys.: Condens. Matter **35**, 333001 (2023).

[10] Q. Wang and Y. D. Chong, Non-Hermitian photonic lattices: Tutorial, J. Opt. Soc. Am. B **40**, 1443 (2023).

[11] N. Okuma and M. Sato, Non-Hermitian Topological Phenomena: A Review, Annu. Rev. Condens. Matter Phys. **14**, 83 (2023).

[12] R. Lin, T. Tai, L. Li, and C. H. Lee, Topological non-Hermitian skin effect, Front. Phys. **18**, 53605 (2023).

[13] L. Zhou and D.-J. Zhang, Non-Hermitian topological phenomena: A review, arXiv:2305.16153.

[14] T. E. Lee, Anomalous Edge State in a Non-Hermitian Lattice, Phys. Rev. Lett. **116**, 133903 (2016).

[15] D. Leykam, K. Y. Bliokh, C. Huang, Y. D. Chong, and F. Nori, Edge Modes, Degeneracies, and Topological Numbers in Non-Hermitian Systems, Phys. Rev. Lett. **118**, 040401 (2017).

[16] H. Shen, B. Zhen, and L. Fu, Topological Band Theory for Non-Hermitian Hamiltonians, Phys. Rev. Lett. **120**, 146402 (2018).

[17] F. K. Kunst, E. Edvardsson, J. C. Budich, and E. J. Bergholtz, Biorthogonal Bulk-Boundary Correspondence in Non-Hermitian Systems, Phys. Rev. Lett. **121**, 026808 (2018).

[18] S. Yao and Z. Wang, Edge States and Topological Invariants of Non-Hermitian Systems, Phys. Rev. Lett. **121**, 086803 (2018).

[19] V. M. Martinez Alvarez, J. E. Barrios Vargas, and L. E. F. Foa Torres, Non-Hermitian robust edge states in one dimension: Anomalous localization and eigenspace condensation at exceptional points, Phys. Rev. B **97**, 121401(R) (2018).

[20] S. Yao, F. Song, and Z. Wang, Non-Hermitian Chern Bands, Phys. Rev. Lett. **121**, 136802 (2018).

[21] C. H. Lee and R. Thomale, Anatomy of skin modes and topology in non-Hermitian systems, Phys. Rev. B **99**, 201103(R) (2019).

[22] H. Zhou and J. Y. Lee, Periodic Table for topological bands with non-Hermitian Bernard-Leclair symmetries, Phys. Rev. B **99**, 235112 (2019).

[23] C.-H. Liu, H. Jiang, and S. Chen, Topological classification of non-Hermitian systems with reflection symmetry, Phys. Rev. B **99**, 125103 (2019).

[24] C. H. Lee, L. Li, and J. Gong, Hybrid Higher-Order Skin-Topological Modes in Non-Reciprocal Systems, Phys. Rev. Lett. **123**, 016805 (2019).

[25] E. Edvardsson, F. K. Kunst, and E. J. Bergholtz, Non-Hermitian extensions of higher-order topological phases and their biorthogonal bulk-boundary correspondence, Phys. Rev. B **99**, 081302(R) (2019).

[26] F. Song, S. Yao, and Z. Wang, Non-Hermitian Skin Effect and Chiral Damping in Open Quantum Systems, Phys. Rev. Lett. **123**, 170401 (2019).

[27] K. Yokomizo and S. Murakami, Bloch Band Theory for Non-Hermitian Systems, Phys. Rev. Lett. **123**, 066404 (2019).

[28] F. Song, S. Yao, and Z. Wang, Non-Hermitian Topological Invariants in Real Space, Phys. Rev. Lett. **123**, 246801 (2019).

[29] K. L. Zhang, H. C. Wu, L. Jin, and Z. Song, Topological phase transition independent of system non-Hermiticity, Phys. Rev. B **100**, 045141 (2019).

[30] T. Liu, Y.-R. Zhang, Q. Ai, Z. Gong, K. Kawabata, M. Ueda, and F. Nori, Second-Order Topological Phases in Non-Hermitian Systems, Phys. Rev. Lett. **122**, 076801 (2019).

[31] H. Wang, J. Ruan, and H. Zhang, Non-Hermitian nodal-line semimetals with an anomalous bulk-boundary correspondence, Phys. Rev. B **99**, 075130 (2019).

[32] L. Herviou, J. H. Bardarson, and N. Regnault, Defining a bulk-edge correspondence for non-Hermitian Hamiltonians via singular-value decomposition, Phys. Rev. A **99**, 052118 (2019).

[33] S. Longhi, Probing non-Hermitian skin effect and non-Bloch phase transitions, Phys. Rev. Res. **1**, 023013 (2019).

[34] S. Longhi, Non-Bloch PT symmetry breaking in non-Hermitian photonic quantum walks, Opt. Lett. **44**, 5804 (2019).

[35] F. K. Kunst and V. Dwivedi, Non-Hermitian systems and topology: A transfer matrix perspective, Phys. Rev. B **99**, 245116 (2019).

[36] K.-I. Imura and Y. Takane, Generalized bulk-edge correspondence for non-Hermitian topological systems, Phys. Rev. B **100**, 165430 (2019).

[37] L. Jin and Z. Song, Bulk-boundary correspondence in non-Hermitian systems in one dimension with chiral inversion symmetry, Phys. Rev. B **99**, 081103(R) (2019).

[38] N. Okuma and M. Sato, Topological Phase Transition Driven by Infinitesimal Instability: Majorana Fermions in Non-Hermitian Spintronics, Phys. Rev. Lett. **123**, 097701 (2019).

[39] J. Y. Lee, J. Ahn, H. Zhou, and A. Vishwanath, Topological Correspondence between Hermitian and Non-Hermitian Systems: Anomalous Dynamics, Phys. Rev. Lett. **123**, 206404 (2019).

[40] D. S. Borgnia, A. J. Kruchkov, and R.-J. Slager, Non-Hermitian Boundary Modes and Topology, Phys. Rev. Lett. **124**, 056802 (2020).

[41] X. Zhang and J. Gong, Non-Hermitian Floquet topological phases: Exceptional points, coalescent edge modes, and the skin effect, Phys. Rev. B **101**, 045415 (2020).

[42] W. Gou, T. Chen, D. Xie, T. Xiao, T.-S. Deng, B. Gadway, W. Yi, and B. Yan, Tunable Nonreciprocal Quantum Transport Through a Dissipative Aharonov-Bohm Ring in Ultracold Atoms, Phys. Rev. Lett. **124**, 070402 (2020).

[43] K. Kawabata, N. Okuma, and M. Sato, Non-Bloch band theory of non-Hermitian Hamiltonians in the symplectic class, Phys. Rev. B **101**, 195147 (2020).

[44] N. Silberstein, J. Behrends, M. Goldstein, and R. Ilan, Berry connection induced anomalous wave-packet dynamics in non-Hermitian systems, Phys. Rev. B **102**, 245147 (2020).

[45] S. Longhi, Non-Bloch-Band Collapse and Chiral Zener Tunneling, Phys. Rev. Lett. **124**, 066602 (2020).

[46] Z. Yang, K. Zhang, C. Fang, and J. Hu, Auxiliary Generalized Brillouin Zone Method in Non-Hermitian Band Theory, Phys. Rev. Lett. **125**, 226402 (2020).

[47] N. Okuma, K. Kawabata, K. Shiozaki, and M. Sato, Topological Origin of Non-Hermitian Skin Effects, Phys. Rev. Lett. **124**, 086801 (2020).

[48] H. Zhao, S. Longhi, and L. Feng, Robust light state by quantum phase transition in non-hermitian optical materials, Sci. Rep. **5**, 17022 (2015).

[49] C. H. Lee and S. Longhi, Ultrafast and anharmonic Rabi oscillations between non-Bloch bands, Commun. Phys. **3**, 147 (2020).

[50] L. Li, C. H. Lee, S. Mu, and J. Gong, Critical non-Hermitian skin effect, Nat. Commun. **11**, 5491 (2020).

[51] G. Shavit and M. Goldstein, Topology by dissipation: Transport properties, Phys. Rev. B **101**, 125412 (2020).

[52] K. Zhang, Z. Yang, and C. Fang, Correspondence between Winding Numbers and Skin Modes in Non-Hermitian Systems, Phys. Rev. Lett. **125**, 126402 (2020).

[53] K. Kawabata, M. Sato, and K. Shiozaki, Higher-order non-Hermitian skin effect, Phys. Rev. B **102**, 205118 (2020).

[54] Y. Fu, J. Hu, and S. Wan, Non-Hermitian second-order skin and topological modes, Phys. Rev. B **103**, 045420 (2021).

[55] R. Okugawa, R. Takahashi, and K. Yokomizo, Second-order topological non-Hermitian skin effects, Phys. Rev. B **102**, 241202(R) (2020).

[56] S. Longhi, Unraveling the non-Hermitian skin effect in dissipative systems, Phys. Rev. B **102**, 201103(R) (2020).

[57] C.-H. Liu, K. Zhang, Z. Yang, and S. Chen, Helical damping and dynamical critical skin effect in open quantum systems, Phys. Rev. Res. **2**, 043167 (2020).

[58] E. Edvardsson, F. K. Kunst, T. Yoshida, and E. J. Bergholtz, Phase transitions and generalized biorthogonal polarization in non-Hermitian systems, Phys. Rev. Res. **2**, 043046 (2020).

[59] P. Gao, M. Willatzen, and J. Christensen, Anomalous Topological Edge States in Non-Hermitian Piezophononic Media, Phys. Rev. Lett. **125**, 206402 (2020).

[60] L. Xiao, T. Deng, K. Wang, G. Zhu, Z. Wang, W. Yi, and P. Xue, Observation of non-Hermitian bulk-boundary correspondence in quantum dynamics, Nat. Phys. **16**, 761 (2020).

[61] A. Ghatak, M. Brandenbourger, J. van Wezel, and C. Coulais, Observation of non-Hermitian topology and its bulk-edge correspondence, Proc. Natl. Acad. Sci. USA **117**, 29561 (2020).

[62] T. Helbig, T. Hofmann, S. Imhof, M. Abdelghany, T. Kiessling, L. W. Molenkamp, C. H. Lee, A. Szameit, M. Greiter, and R. Thomale, Generalized bulk-boundary correspondence in non-Hermitian topolectrical circuits, Nat. Phys. **16**, 747 (2020).

[63] T. Hofmann, T. Helbig, F. Schindler, N. Salgo, M. Brzezinska, M. Greiter, T. Kiessling, D. Wolf, A. Vollhardt, A. Kabasi, C. H. Lee, A. Bilusic, R. Thomale, and T. Neupert, Reciprocal skin effect and its realization in a topolectrical circuit, Phys. Rev. Res. **2**, 023265 (2020).

[64] S. Weidemann, M. Kremer, T. Helbig, T. Hofmann, A. Stegmaier, M. Greiter, R. Thomale, and A. Szameit, Topological funneling of light, Science **368**, 311 (2020).

[65] Y. Song, W. Liu, L. Zheng, Y. Zhang, B. Wang, and P. Lu, Two-dimensional non-Hermitian Skin Effect in a Synthetic Photonic Lattice, Phys. Rev. Appl. **14**, 064076 (2020).

[66] H. Hu and E. Zhao, Knots and Non-Hermitian Bloch Bands, Phys. Rev. Lett. **126**, 010401 (2021).

[67] K. Kawabata, K. Shiozaki, and S. Ryu, Topological Field Theory of Non-Hermitian Systems, Phys. Rev. Lett. **126**, 216405 (2021).

[68] K. Yokomizo and S. Murakami, Non-Bloch band theory in bosonic Bogoliubov-de Gennes systems, Phys. Rev. B **103**, 165123 (2021).

[69] X. Zhang, Y. Tian, J.-H. Jiang, M.-H. Lu, and Y.-F. Chen, Observation of higher-order non-Hermitian skin effect, Nat. Commun. **12**, 5377 (2021).

[70] S. Longhi, Non-Hermitian skin effect beyond the tight-binding models, Phys. Rev. B **104**, 125109 (2021).

[71] S. Longhi, Non-Hermitian topological mobility edges and transport in photonic quantum walks, Opt. Lett. **47**, 2951 (2022).

[72] S. Longhi, Self-Healing of Non-Hermitian Topological Skin Modes, Phys. Rev. Lett. **128**, 157601 (2022).

[73] W.-T. Xue, Y.-M. Hu, F. Song, and Z. Wang, Non-Hermitian Edge Burst, Phys. Rev. Lett. **128**, 120401 (2022).

[74] S. Longhi, Non-Hermitian skin effect and self-acceleration, Phys. Rev. B **105**, 245143 (2022).

[75] Q. Liang, D. Xie, Z. Dong, H. Li, H. Li, B. Gadway, W. Yi, and B. Yan, Dynamic Signatures of Non-Hermitian Skin Effect and Topology in Ultracold Atoms, Phys. Rev. Lett. **129**, 070401 (2022).

[76] R. Yang, J. W. Tan, T. Tai, J. M. Koh, L. Li, S. Longhi, and C. H. Lee, Designing non-Hermitian real spectra through electrostatics, Sci. Bull. **67**, 1865 (2022).

[77] Y. Li, X. Ji, Y. Chen, X. Yan, and X. Yang, Topological energy braiding of non-Bloch bands, Phys. Rev. B **106**, 195425 (2022).

[78] Z. Gu, H. Gao, H. Xue, J. Li, Z. Su, and J. Zhu, Transient non-Hermitian skin effect, Nat. Commun. **13**, 7668 (2022).

[79] K. Zhang, Z. Yang, and C. Fang, Universal non-Hermitian skin effect in two and higher dimensions, Nat. Commun. **13**, 2496 (2022).

[80] W. Wang, X. Wang, and G. Ma, Non-Hermitian morphing of topological modes, Nature (London) **608**, 50 (2022).

[81] Z. Ou, Y. Wang, and L. Li, Non-Hermitian boundary spectral winding, Phys. Rev. B **107**, L161404 (2023).

[82] S. Longhi, Phase transitions in non-Hermitian superlattices, Phys. Rev. B **107**, 134203 (2023).

[83] K. Yokomizo and S. Murakami, Non-Bloch bands in two-dimensional non-Hermitian systems, Phys. Rev. B **107**, 195112 (2023).

[84] S. Longhi and L. Feng, Complex Berry phase and imperfect non-Hermitian phase transitions, Phys. Rev. B **107**, 085122 (2023).

[85] Y. Fu and Y. Zhang, Anatomy of open-boundary bulk in multiband non-Hermitian systems, Phys. Rev. B **107**, 115412 (2023).

[86] A. Jazaeri and I. I. Satija, Localization transition in incommensurate non-Hermitian systems, Phys. Rev. E **63**, 036222 (2001).

[87] Q.-B. Zeng, S. Chen, and R. Lü, Anderson localization in the non-Hermitian Aubry-André-Harper model with physical gain and loss, Phys. Rev. A **95**, 062118 (2017).

[88] S. Longhi, Topological Phase Transition in Non-Hermitian Quasicrystals, Phys. Rev. Lett. **122**, 237601 (2019).

[89] S. Longhi, Metal-insulator phase transition in a non-Hermitian Aubry-André-Harper model, Phys. Rev. B **100**, 125157 (2019).

[90] Y. Liu, X.-P. Jiang, J. Cao, and S. Chen, Non-Hermitian mobility edges in one-dimensional quasicrystals with parity-time symmetry, Phys. Rev. B **101**, 174205 (2020).

[91] Q.-B. Zeng, Y.-B. Yang, and Y. Xu, Topological phases in non-Hermitian Aubry-André-Harper models, Phys. Rev. B **101**, 020201(R) (2020).

[92] Q.-B. Zeng and Y. Xu, Winding numbers and generalized mobility edges in non-Hermitian systems, Phys. Rev. Res. **2**, 033052 (2020).

[93] T. Liu, H. Guo, Y. Pu, and S. Longhi, Generalized Aubry-André self-duality and mobility edges in non-Hermitian quasi-periodic lattices, Phys. Rev. B **102**, 024205 (2020).

[94] S. Longhi, Anderson localization in dissipative lattices, Annalen der Physik **535**, 2200658 (2023).

[95] X. Cai, Boundary-dependent self-dualities, winding numbers, and asymmetrical localization in non-Hermitian aperiodic one-dimensional models, Phys. Rev. B **103**, 014201 (2021).

[96] Y. Liu, Q. Zhou, and S. Chen, Localization transition, spectrum structure and winding numbers for one-dimensional non-Hermitian quasicrystals, Phys. Rev. B **104**, 024201 (2021).

[97] Y. Liu, Y. Wang, X.-J. Liu, Q. Zhou, and S. Chen, Exact mobility edges, PT-symmetry breaking and skin effect in one-dimensional non-Hermitian quasicrystals, Phys. Rev. B **103**, 014203 (2021).

[98] J. Claes and T. L. Hughes, Skin effect and winding number in disordered non-Hermitian systems, Phys. Rev. B **103**, L140201 (2021).

[99] L.-Z. Tang, G.-Q. Zhang, L.-F. Zhang, and D.-W. Zhang, Localization and topological transitions in non-Hermitian quasiperiodic lattices, Phys. Rev. A **103**, 033325 (2021).

[100] S. Longhi, Phase transitions in a non-Hermitian Aubry-André-Harper model, Phys. Rev. B **103**, 054203 (2021).

[101] K. Kawabata and S. Ryu, Nonunitary Scaling Theory of Non-Hermitian Localization, Phys. Rev. Lett. **126**, 166801 (2021).

[102] R. Sarkar, S. S. Hegde, and A. Narayan, Interplay of disorder and point-gap topology: Chiral modes, localization, and non-Hermitian Anderson skin effect in one dimension, Phys. Rev. B **106**, 014207 (2022).

[103] L.-J. Zhai, G.-Y. Huang, and S. Yin, Nonequilibrium dynamics of the localization-delocalization transition in the non-Hermitian Aubry-André model, Phys. Rev. B **106**, 014204 (2022).

[104] S. Longhi, Non-Hermitian Maryland model, Phys. Rev. B **103**, 224206 (2021).

[105] L. Zhou and Y. Gu, Topological delocalization transitions and mobility edges in the nonreciprocal Maryland model, J. Phys.: Condens. Matter **34**, 115402 (2022).

[106] X. Cai, Localization transitions and winding numbers for non-Hermitian Aubry-André-Harper models with off-diagonal modulations, Phys. Rev. B **106**, 214207 (2022).

[107] W. Han and L. Zhou, Dimerization-induced mobility edges and multiple reentrant localization transitions in non-Hermitian quasicrystals, Phys. Rev. B **105**, 054204 (2022).

[108] Q. Lin, T. Li, L. Xiao, K. Wang, W. Yi, and P. Xue, Observation of non-Hermitian topological Anderson insulator in quantum dynamics, Nat. Commun. **13**, 3229 (2022).

[109] S. Weidemann, M. Kremer, S. Longhi, and A. Szameit, Topological triple phase transition in non-Hermitian Floquet quasicrystals, Nature (London) **601**, 354 (2022).

[110] Q. Lin, T. Li, L. Xiao, K. Wang, W. Yi, and P. Xue, Topological Phase Transitions and Mobility Edges in Non-Hermitian Quasicrystals, Phys. Rev. Lett. **129**, 113601 (2022).

[111] S. Aubry and G. André, Analyticity breaking and Anderson localization in incommensurate lattices, Ann. Israel Phys. Soc. **3**, 133 (1980).

[112] E. Lee, H. Lee, and B.-J. Yang, Many-body approach to non-Hermitian physics in fermionic systems, Phys. Rev. B **101**, 121109(R) (2020).

[113] A. Panda and S. Banerjee, Entanglement in nonequilibrium steady states and many-body localization breakdown in a current-driven system, Phys. Rev. B **101**, 184201 (2020).

[114] S. Lieu, Non-Hermitian Majorana modes protect degenerate steady state, Phys. Rev. B **100**, 085110 (2019).

[115] N. Matsumoto, K. Kawabata, Y. Ashida, S. Furukawa, and M. Ueda, Continuous Phase Transition without Gap Closing in Non-Hermitian Quantum Many-Body Systems, Phys. Rev. Lett. **125**, 260601 (2020).

[116] A. Banerjee, S. S. Hegde, A. Agarwala, and A. Narayan, Chiral metals and entrapped insulators in a one-dimensional topological non-Hermitian system, Phys. Rev. B **105**, 205403 (2022).

[117] F. Alsallom, L. Herviou, O. V. Yazyev, and M. Brzezinska, Fate of the non-Hermitian skin effect in many-body fermionic systems, Phys. Rev. Res. **4**, 033122 (2022).

[118] N. Okuma and M. Sato, Quantum anomaly, non-Hermitian skin effects, and entanglement entropy in open systems, Phys. Rev. B **103**, 085428 (2021).

[119] K. Kawabata, T. Numasawa, and S. Ryu, Entanglement Phase Transition Induced by the Non-Hermitian Skin Effect, Phys. Rev. X **13**, 021007 (2023).

[120] X. Turkeshi and M. Schiró, Entanglement and correlation spreading in non-Hermitian spin chains, Phys. Rev. B **107**, L020403 (2023).

[121] K. Li, Z.-C. Liu, and Y. Xu, Entanglement phase transitions in disordered non-Hermitian systems, arXiv:2305.12342.

[122] J. Liu and Z. Xu, From ergodicity to many-body localization in a one-dimensional interacting non-Hermitian stark system, arXiv:2305.13636.

[123] T. Fukui and N. Kawakami, Breakdown of the Mott insulator: Exact solution of an asymmetric Hubbard model, Phys. Rev. B **58**, 16051 (1998).

[124] R. Hamazaki, K. Kawabata, and M. Ueda, Non-Hermitian Many-Body Localization, Phys. Rev. Lett. **123**, 090603 (2019).

[125] T. Liu, J. J. He, T. Yoshida, Z.-L. Xiang, and F. Nori, Non-Hermitian topological Mott insulators in one-dimensional fermionic superlattices, Phys. Rev. B **102**, 235151 (2020).

[126] L.-J. Zhai, S. Yin, and G.-Y. Huang, Many-body localization in a non-Hermitian quasi-periodic system, Phys. Rev. B **102**, 064206 (2020).

[127] S.-B. Zhang, M. M. Denner, T. Bzdusek, M. A. Sentef, and T. Neupert, Symmetry breaking and spectral structure of the interacting Hatano-Nelson model, Phys. Rev. B **106**, L121102 (2022).

[128] K. Kawabata, K. Shiozaki, and S. Ryu, Many-body topology of non-Hermitian systems, Phys. Rev. B **105**, 165137 (2022).

[129] D.-W. Zhang, Y.-L. Chen, G.-Q. Zhang, L.-J. Lang, Z. Li, and S.-L. Zhu, Skin superfluid, topological Mott insulators, and asymmetric dynamics in an interacting non-Hermitian Aubry-André-Harper model, Phys. Rev. B **101**, 235150 (2020).

[130] S. Ghosh, S. Gupta, and M. Kulkarni, Spectral properties of disordered interacting non-Hermitian systems, Phys. Rev. B **106**, 134202 (2022).

[131] T. Orito and K.-I. Imura, Unusual wave-packet spreading and entanglement dynamics in non-Hermitian disordered many-body systems, Phys. Rev. B **105**, 024303 (2022).

[132] K. Suthar, Y.-C. Wang, Y.-P. Huang, H. H. Jen, and J.-S. You, Non-Hermitian many-body localization with open boundaries, Phys. Rev. B **106**, 064208 (2022).

[133] T. Yoshida and Y. Hatsugai, Reduction of one-dimensional non-Hermitian point-gap topology by interactions, Phys. Rev. B **106**, 205147 (2022).

[134] R. Shen and C. H. Lee, Non-Hermitian skin clusters from strong interactions, Commun. Phys. **5**, 238 (2022).

[135] T. Yoshida and Y. Hatsugai, Fate of exceptional points under interactions: Reduction of topological classifications, Phys. Rev. B **107**, 075118 (2023).

[136] L. Mao, Y. Hao, and L. Pan, Non-Hermitian skin effect in a one-dimensional interacting Bose gas, Phys. Rev. A **107**, 043315 (2023).

[137] Y.-C. Wang, K. Suthar, H. H. Jen, Y.-T. Hsu, and J.-S. You, Non-Hermitian skin effects on many-body localized and thermal phases, Phys. Rev. B **107**, L220205 (2023).

[138] H.-Z. Li, X.-J. Yu, and J.-X. Zhong, Non-Hermitian stark many-body localization, arXiv:2305.09387.

[139] S. Hamanaka, K. Yamamoto, and T. Yoshida, Interaction-induced Liouvillian skin effect in a fermionic chain with two-body loss, arXiv:2305.19697.

[140] K. Winkler, G. Thalhammer, F. Lang, R. Grimm, J. Hecker Denschlag, A. J. Daley, A. Kantian, H. P. Büchler, and P. Zoller, Repulsively bound atom pairs in an optical lattice, Nature (London) **441**, 853 (2006).

[141] M. Valiente and D. Petrosyan, Two-particle states in the Hubbard model, J. Phys. B **41**, 161002 (2008).

[142] N. Strohmaier, D. Greif, R. Jördens, L. Tarruell, H. Moritz, T. Esslinger, R. Sensarma, D. Pekker, E. Altman, and E. Demler, Observation of Elastic Doublon Decay in the Fermi-Hubbard Model, Phys. Rev. Lett. **104**, 080401 (2010).

[143] F. Hofmann and M. Potthoff, Doublon dynamics in the extended Fermi-Hubbard model, Phys. Rev. B **85**, 205127 (2012).

[144] A. L. Chudnovskiy, D. M. Gangardt, and A. Kamenev, Doublon Relaxation in the Bose-Hubbard Model, Phys. Rev. Lett. **108**, 085302 (2012).

[145] S. Longhi and G. Della Valle, Low-energy doublons in the ac-driven two-species Hubbard model, Phys. Rev. A **87**, 013634 (2013).

[146] L. Xia, L. A. Zundel, J. Carrasquilla, A. Reinhard, J. M. Wilson, M. Rigol, and D. S. Weiss, Quantum distillation and confinement of vacancies in a doublon sea, Nat. Phys. **11**, 316 (2015).

[147] K. Balzer, M. Rodriguez Rasmussen, N. Schlünzen, J.-P. Joost, and M. Bonitz, Doublon Formation by Ions Impacting a Strongly Correlated Finite Lattice System, Phys. Rev. Lett. **121**, 267602 (2018).

[148] S. Trotzky, P. Cheinet, S. Fölling, M. Feld, U. Schnorrberger, A. M. Rey, A. Polkovnikov, E. A. Demler, M. D. Lukin, and I. Bloch, Time-resolved observation and control of superexchange interactions with ultracold atoms in optical lattices, Science **319**, 295 (2008).

[149] Y.-A. Chen, S. Nascimbene, M. Aidelsburger, M. Atala, S. Trotzky, and I. Bloch, Controlling Correlated Tunneling and Superexchange Interactions with AC-Driven Optical Lattices, Phys. Rev. Lett. **107**, 210405 (2011).

[150] M. Schreiber, S. S. Hodgman, P. Bordia, H. P. Lüschen, M. H. Fischer, R. Vosk, E. Altman, U. Schneider, and I. Bloch, Observation of many-body localization of interacting fermions in a quasirandom optical lattice, Science **349**, 842 (2015).

[151] P. M. Preiss, R. Ma, M. E. Tai, A. Lukin, M. Rispoli, P. Zupancic, Y. Lahini, R. Islam, and M. Greiner, Strongly correlated quantum walks in optical lattices, Science **347**, 1229 (2015).

[152] I. S. Besedin, M. A. Gorlach, N. N. Abramov, I. Tsitsilin, I. N. Moskalenko, A. A. Dobronosova, D. O. Moskalev, A. R. Matanin, N. S. Smirnov, I. A. Rodionov, A. N. Poddubny, and A. V. Ustinov, Topological excitations and bound photon pairs in a superconducting quantum metamaterial, Phys. Rev. B **103**, 224520 (2021).

[153] G. Corrielli, A. Crespi, G. Della Valle, S. Longhi, and R. Osellame, Fractional Bloch oscillations in photonic lattices, Nat. Commun. **4**, 1555 (2013).

[154] N. A. Olekhno, E. I. Kretov, A. A. Stepanenko, P. A. Ivanova, V. V. Yaroshenko, E. M. Puhtina, D. S. Filonov, B. Cappello, L. Matekovits, and M. A. Gorlach, Topological edge states of interacting photon pairs emulated in a topolectrical circuit, Nat. Commun. **11**, 1436 (2020).

[155] W. Zhang, F. Di, H. Yuan, H. Wang, X. Zheng, L. He, H. Sun, and X. Zhang, Observation of non-Hermitian aggregation effects induced by strong interactions, Phys. Rev. B **105**, 195131 (2022).

[156] D. Jaksch, C. Bruder, J. I. Cirac, C. W. Gardiner, and P. Zoller, Cold Bosonic Atoms in Optical Lattices, Phys. Rev. Lett. **81**, 3108 (1998).

[157] N. Hatano and D. R. Nelson, Localization Transitions in Non-Hermitian Quantum Mechanics, Phys. Rev. Lett. **77**, 570 (1996).

[158] S. Longhi, Spectral structure and doublon dissociation in the two-particle non-Hermitian Hubbard model (unpublished).